NASA Technical Memorandum 109070

DYNAMIC ANAYLSIS OF PRETWISTED ELASTICALLY-COUPLED ROTOR BLADES

Mark W. Nixon and Howard E. Hinnant
Vehicle Structures Directorate, U.S. Army Research Laboratory,
Langley Research Center, Hampton, Virginia

January 1994

National Aeronautics and
Space Administration
Langley Research Center
Hampton, Virginia 23681-0001

DYNAMIC ANALYSIS OF PRETWISTED ELASTICALLY-COUPLED ROTOR BLADES

Mark W. Nixon*
Howard E. Hinnant†
U.S. Army Vehicle Structures Directorate
NASA Langley Research Center
Hampton, VA 23681

ABSTRACT

This paper addresses the accuracy of using a one-dimensional analysis to predict frequencies of elastically-coupled highly-twisted rotor blades. Degrees of freedom associated with shear deformation are statically condensed from the formulation, so the analysis uses only those degrees of freedom associated with classical beam theory. The effects of cross section deformation (warping) are considered, and are shown to become significant for some types of elastic coupling. Improved results are demonstrated for highly-coupled blade structures through account of warping in a local cross section analysis, without explicit inclusion of these effects in the beam analysis. A convergence study is also provided which investigates the potential for improving efficiency of elastically-coupled beam analysis through implementation of a p-version beam finite element.

INTRODUCTION

There is a potential for improving the performance, aeroelastic stability, and vibration characteristics of rotorcraft through the use of elastically-coupled composite rotor blades. A complete analysis of such systems requires use of comprehensive aeroelastic codes that, due to their complexity and size, are in practice limited to modeling the elastic rotor blade with a one-dimensional theory. One primary function of any aeroelastic code is to perform an accurate dynamic analysis of the rotating blade in a vacuum. The accuracy of this part of the analysis may be questionable with the presence of elastic couplings because nonclassical beam effects, which are generally ignored, may become important for these structures.

Many past studies have investigated the capabilities of one-dimensional analysis in predicting behavior of elastically-coupled composite beams. Smith and Chopra (1991), Rehfield (1990), and Nixon (1989) showed the importance of nonclassical effects such as transverse shear deformation and warping in the *static* behavior of these structures. The influences of shear deformation and warping in nonrotating *dynamic* analysis of coupled beams have been investigated by Kosmatka (1988) and Kosmatka and Ie (1991). These studies demonstrated the importance of out-of-plane shear-dependent warping and in-plane warping (anticlastic deformations) in the free-vibration analysis of beams in which shear deformation has significant effects, such as the bending frequencies of short beams and higher modes of long beams. Shear deformation also is an important consideration for beams with some types of elastic couplings, such as bending-shear elastic coupling. Based on the work of Kosmatka and Ie (1991), it appears necessary to include the shear-related warping effects for an accurate prediction of frequencies of bending-shear coupled beams.

The effects of shear deformation on *rotating* beam dynamics were examined by Smith and Chopra (1992) in a study which extended the rotor analysis known as UMARC (University of Maryland Advanced Rotor Code, Hong and Chopra 1985a,1985b) to include explicit shear degrees of freedom. Results of this study showed improvements in the prediction of lower mode frequencies for bending-shear coupled beams. It is clear from this study that shear deformation effects must be included in the beam analysis to obtain accurate frequencies of bending-shear coupled beams, but the approach of using explicit shear degrees of freedom increased the size and complexity of the formulation. This is undesirable in a comprehensive code because the additional degrees of freedom must be addressed in the aerodynamic models as well.

The formulation for *rotating* beams is more involved than that for nonrotating beams because the rotation effects can only be included through use of the geometrically nonlinear theory of elasticity. For a general anisotropic beam, accounting for all the possible nonclassical beam effects in a nonlinear formulation is undesirable because of size and complexity considerations. One possible approach for simplifying the formulation is to split the equations associated with the geometrically nonlinear three-dimensional theory of elasticity into a nonlinear one-dimensional set of equations and a linear two-dimensional set of equations. This approach has theoretically been shown appropriate for twisted nonhomogeneous anisotropic blades through use of a variational-asymptotical method by Hodges and Atilgan (1991). An explicit formulation of this approach is proposed which considers the influence of nonclassical effects only on the effective beam stiffness properties and eliminates degrees of freedom associated with shear deformation through static condensation. This formulation leads to a rotating beam analysis based on only those degrees of freedom which have been used for classical beam analyses. A second analysis, which should consider all the possible nonclassical influences, but may be based on linear theory, is used to determine the effective beam properties for the first analysis. If such an approach is accurate for geometries and materials typical of rotor blades, then rotor analyses based on isotropic materials and classical beam theory may be modified to incorporate composite materials and non-

*Aerospace Engineer, AHS member
†Aerospace Engineer, AIAA member

classical effects.

This paper will address the accuracy of using one-dimensional analysis for the prediction of rotating beam frequencies of elastically-coupled, highly twisted rotor blades. There are three objectives for this study: 1) show that the degrees of freedom associated with shear deformation may be statically condensed from the analysis, 2) show that the nonclassical influences associated with cross section warping, which may become significant as a result of elastic coupling, can be accounted for without the incorporation of these effects explicitly in the rotating beam analysis, and 3) determine the potential improvement in efficiency by using higher-order displacement approximations in a finite element implementation.

A rotating beam analysis was developed based on a formulation of nonlinear equations of motion and a finite element implementation. The formulation is derived in Appendix A to show how shear deformation and warping enter the theory. The formulation is nonlinear as is required to capture the centrifugal stiffening effects even in the linearized form of the equations. The degrees of freedom associated with shear deformation were eliminated through static condensation of the linear force-displacement relationships. The linear part of the formulation was implemented as a p-version beam finite element such that the degree of polynomial approximation for the bending, torsion, and axial displacements may be independently selected. This implementation is described in Appendix B along with the results of a convergence study. This convergence study shows the efficiency of certain displacement approximations for a bending-twist-coupled beam.

Results of the present rotating beam analysis are compared with those produced by Smith and Chopra (1992) for a set of elastically-coupled rotor blades to show that static condensation of the shear degrees of freedom is valid for the modes considered. Attention is then focused on nonclassical effects (shear deformation and warping) and their influence on the prediction of both rotating and nonrotating frequencies for elastically-coupled and highly twisted beams. Comparisons are made with experimental results obtained by Chandra (1988), 1-D analytical results obtained with UMARC as presented by Smith and Chopra (1992), and 3-D analytical results obtained using the analysis of Hinnant (1992).

FORMULATION

For this formulation, the blade is assumed to be a long and slender beam, and constructed from anisotropic materials such that displacement modes may be elastically coupled. The blade may deform in extension u_e, lag bending v, flap bending w, and torsion ϕ, and both built-in pretwist and elastic twist deformation may be large. The equations of motion are formulated based on the form of Hamilton's variational principal typically used in rotor analysis,

$$\delta\Pi = \int_{t_1}^{t_2} (\delta U - \delta T - \delta W)\, dt = 0 \qquad (1)$$

The potential energy variation δU is developed entirely by the elastic strain of deformation, the kinetic energy variation δT is developed from blade velocity terms, and the work variation δW is zero in the present formulation (no external loading is considered, the system is conservative).

Strain Energy Formulation

The elastic strain energy is derived in Appendix A. Only the linear contribution to the strain energy variational is of interest in the present study, which is given by

$$\delta U_{lin} = \int_0^R \delta\hat{v}_i \mathrm{k}_{ij} \hat{v}_j \, dx \qquad (2)$$

where $(i, j = 1, 9)$, and

$$\delta\hat{v}_i = \{\ \delta u_e'\ \ \delta v_s'\ \ \delta w_s'\ \ \delta\phi\ \ \delta\phi'\ \ \delta w'\ \ \delta w''\ \ \delta v'\ \ \delta v''\ \} \qquad (3)$$

and k_{ij} is a 9x9 cross section stiffness matrix. The fourth, sixth, and eighth rows and columns of k_{ij} are zeros because the strain energy terms associated with $\delta\phi$, $\delta w'$, and $\delta v'$ are nonlinear. The linear stiffness matrix k_{ij} can thus be reduced to a 6x6 coupled stiffness matrix with diagonal stiffnesses corresponding to an axial stiffness, two shear stiffnesses, a torsional stiffness, and two bending stiffnesses. For a static problem, the force-displacement relationship is given by:

$$\begin{bmatrix} Q_x \\ Q_y \\ Q_z \\ M_x \\ -M_y \\ M_z \end{bmatrix} = [\mathrm{k}_{ij}] \begin{bmatrix} u_e' \\ v_s' \\ w_s' \\ \phi' \\ w'' \\ v'' \end{bmatrix} \qquad (4)$$

where Q are forces in the directions indicated by subscripts and M are moments about directions indicated by subscripts. This relationship may be simplified for beam behavior by eliminating the shear-related degrees of freedom from the relationship. As was shown by Hodges *et al.* (1987) it is proper to assume the shear forces associated with the shear deformation are zero, but not the shear strains because of the presence of coupling terms. With Q_y and Q_z set to zero, the shear deformations may be removed through static condensation. This amounts to eliminating the rows and columns associated with shear from the compliance matrix rather than from the stiffness matrix. The compliance matrix is formulated by inverting the 6x6 cross section stiffness matrix,

$$S_{ij} = k_{ij}^{-1}$$

and after elimination of the second and third rows and columns may be written as

$$\begin{bmatrix} u_e' \\ \phi' \\ w'' \\ v'' \end{bmatrix} = [S_{ij}'] \begin{bmatrix} Q_x \\ M_x \\ -M_y \\ M_z \end{bmatrix} \qquad (5)$$

The bending-related compliance terms include the flexibility associated with any shear coupling present in the cross section. The 4x4 compliance matrix is then inverted to obtain the desired 4x4 form of the fully coupled cross section stiffness matrix k_{ij}', which implicitly includes shear deformation effects. The term k_{ij} is thus

replaced by k'_{ij} in Eqn. 2, and the vector of continuous displacements is reduced to

$$\delta\hat{v}_i = \{ \ \delta u'_e \quad \delta\phi' \quad \delta w'' \quad \delta v'' \ \} \tag{6}$$

This stiffness matrix is applicable to the dynamic problem assuming the dynamic effects associated with shear deformation are small.

Kinetic Energy Formulation

For completeness, the kinetic energy is also derived in Appendix A. As was the case for the strain energy, only the linear contribution to the kinetic energy variational is of interest in the present study, and is given by

$$\delta T_{lin} = \int_0^R \delta\hat{u}_i \{ m_{ij}\ddot{\hat{u}}_j + c_{ij}\dot{\hat{u}}_j + k_{ij}\hat{u}_j \} \, dx \tag{7}$$

with the vector of displacement variations for the kinetic energy formulation given by,

$$\delta\hat{u}_i = \{ \ \delta u_e \quad \delta v \quad \delta v' \quad \delta w \quad \delta w' \quad \delta\phi \ \} \tag{8}$$

m_{ij} is the mass matrix which includes rotational inertias, c_{ij} is the linear damping matrix which is zero in the absence of precone (β_P), and k_{ij} contains the centrifugal stiffening terms which are of nonlinear origin.

Implementation

The linear parts of the strain and kinetic energies defined in Eqns. 2 and 7 were used to develop a p-version beam finite element so that the degree of polynomial approximation for the bending, torsion, and axial displacements may be independently selected. Integrations over the element length were performed symbolically to increase computational efficiency of the analysis. Further description of the beam element formulation is provided in Appendix B. The final form of the rotating blade equations after application of Hamilton's principle in discretized form is given by

$$M_{ij}\ddot{q}_j + C_{ij}\dot{q}_j + K_{ij}q_j = 0 \tag{9}$$

where M_{ij}, C_{ij}, and K_{ij} are the element mass, damping, and stiffness matrices, respectively. q_j represents the vector of discrete displacements. The elements are assembled to form a global system which is solved using standard eigenvalue techniques to obtain modes and frequencies.

APPLICATION

The capabilities and limitations of the present analysis with respect to mode and frequency predictions of highly-twisted elastically-coupled beams are examined. The present analysis, referred to as CORBA (COmposite Rotating Beam Analysis) for clarity, is first verified for simple cases where the elastic coupling influences are small. The predictions of CORBA are then examined for cases where the elastic coupling effects become significant. Convergence of the CORBA results was achieved using five beam elements with cubic polynomials for the bending displacements, and quadratic polynomials for the axial and torsion displacements. These approximations gave convergence in the most highly twisted rotating beams considered in this study, and were more than adequate for the untwisted cases.

Table 1: Composite blade stiffnesses for *Series 1*.

Stiffness	Baseline	Sym.	Anti-Sym.
$EA/m_0\Omega^2R^2$	378.1	378.1	378.1
$GA_y/m_0\Omega^2R^2$	50.77	50.43	50.77
$GA_z/m_0\Omega^2R^2$	25.85	25.85	25.85
$GJ/m_0\Omega^2R^4$	.003822	.003815	.003796
$EI_y/m_0\Omega^2R^4$	.008345	.008345	.008345
$EI_z/m_0\Omega^2R^4$	.023198	.023198	.023198
$k_{12}/m_0\Omega^2R^2$	0	-33.67	0
$k_{13}/m_0\Omega^2R^2$	0	0	0
$k_{14}/m_0\Omega^2R^3$	0	0	.3589
$k_{25}/m_0\Omega^2R^3$	0	0	-.1794
$k_{36}/m_0\Omega^2R^3$	0	0	.1796
$k_{45}/m_0\Omega^2R^4$	0	-.001311	0
$k_{46}/m_0\Omega^2R^4$	0	0	0

Table 2: Frequencies for the *Series 1* baseline.

CORBA (per rev)	UMARC (per rev)	Diff. (%)	Pred. Mode
0.749	0.747	0.23	1st lag
1.147	1.146	0.09	1st flap
3.398	3.389	0.26	2nd flap
4.338	4.315	0.53	2nd lag
4.590	4.590	0.01	1st tor.
7.459	7.416	0.58	3rd flap
13.61	13.60	0.08	2nd tor.

Table 3: Frequencies for the *Series 1* symmetric case.

CORBA (per rev)	UMARC (per rev)	Diff. %	Pred. Mode
0.749	0.747	0.23	1st lag
1.143	1.142	0.11	1st flap
3.354	3.346	0.25	2nd flap
4.338	4.314	0.55	2nd lag
4.590	4.590	0.01	1st tor.
13.63	13.62	0.08	2nd tor.

Table 4: Frequencies for the *Series 1* anti-symmetric case.

CORBA (per rev)	UMARC (per rev)	Diff. %	Pred. Mode
0.736	0.735	0.08	1st lag
1.142	1.141	0.07	1st flap
3.344	3.389	1.35	2nd flap
4.256	4.244	0.29	2nd lag
4.367	4.367	0.01	1st tor.

Analysis Verification

Several cases were studied to verify CORBA predictions of modes and frequencies for rotating composite blades. Three of the case studies are presented in this paper. These three configurations, referred to as *Series 1*, were developed by Smith and Chopra (1992) to investigate the effects of elastically coupled rotor blades

Table 5: Rotating frequencies of the *Series 2* anti-symmetric case at $\Omega = 1002$ RPM.

CORBA (Hz)	UMARC (Hz)	UMARC* (Hz)	Experiment (Hz)	CORBA† Diff. (%)	UMARC*† Diff. (%)	Pred. Mode
36.53	36.49	43.52	33.6	8.70	29.5	1st flap
53.89	53.73	62.57	46.6	15.65	34.3	1st lag
202.8	202.2	247.8	184.0	10.2	34.7	2nd flap
336.4	328.2	383.6				2nd lag
493.6	493.7	493.7				1st tor.

† Correlation with experimental results. * UMARC without shear deformation.

for a soft-inplane hingeless rotor helicopter. The blade cross section was designed to be representative of an actual rotor system with respect to stiffness and inertial properties. The main structural member of the rotor blade was a single cell composite box beam. The ply orientation of the box beam laminates was adjusted to produce the three configurations considered here. The first case is uncoupled (baseline), the second is extension-flap shear, flap bending-twist coupled (symmetric case), and the third is bending-shear, extension-twist coupled (anti-symmetric case). The terms "symmetric" and "anti-symmetric" refer to the orientation of laminates with respect to the bending axes of the box beam, but not to the laminates themselves. The individual laminates themselves are arranged in a symmetric configuration for all cases. The stiffness properties associated with each case, as reported by Smith and Chopra (1992), are shown in Table 1. In this table, EA is the axial stiffness, GA_y and GA_z are the lag and flap shear stiffnesses, GJ is the torsional stiffness, and EI_y and EI_z are the flap and lag bending stiffnesses. k_{12} represents the extension-flap shear coupling, k_{13} the extension-lag shear coupling, k_{14} the extension-twist coupling, k_{25} the lag shear-flap bending coupling, k_{36} the flap shear-lag bending coupling, k_{45} the flap bending-twist coupling, and finally k_{46} the lag bending-twist coupling. All the stiffnesses are shown to be nondimensionalized by appropriate factors of m_0 the mass per unit length, Ω the reference rotational velocity, and R the blade radius.

The rotating natural frequencies for each case as predicted by two analyses, UMARC and CORBA, are shown in Tables 2-4. All references to "UMARC" are understood to mean the version which has a 19 degree-of-freedom shear deformable beam element, unless otherwise indicated. The difference in predictions between CORBA and UMARC is shown to be less than one percent for all modes except the second flap mode of the anti-symmetric case where the difference is 1.35 percent. Comparisons studies, not shown here, also showed good agreement between the two analyses for highly twisted blades, up to 90°. These correlations indicate that the present analysis has accurately captured the effects of rotation, twist, elastic coupling, and shear deformation.

Two more case studies, designated *Series 2*, were examined to determine the influence of higher amounts of elastic coupling on the frequency predictions of UMARC and CORBA. The cross section geometry of these cases was a simple single cell box beam, without any nonstructural mass or secondary structure, and in one case the layup was arranged in an anti-symmetric configuration while the other was arranged in a symmetric configuration. The symmetric case had a $[15]_6$ layup of graphite epoxy material on the top and bottom walls while the sides had a layup of $[15/\text{-}15]_3$. The anti-symmetric layup was $[15]_6$ on top and $[\text{-}15]_6$ on the bottom wall, and one side was $[15]_6$ while the other side was $[\text{-}15]_6$. The box had an outside width of .953 inches and outside depth of .537 inches, and the specimens were 33.25 inches long. These cases were examined because a set of experimental results, presented by Chandra and Chopra (1989), was available for correlation with the analytical predictions.

The cross section mass and stiffness properties of these specimens were calculated using a two-dimensional analysis described in detail by Smith and Chopra (1990). This analysis accounts for shear deformation and the out-of-plane warping associated with torsion, but does not consider any other warping effects. The mass and stiffness properties developed by this analysis were used as input to both UMARC and CORBA.

The analytical and experimental results are listed in Table 5 for the anti-symmetric case and in Table 6 for the symmetric case. The importance of including the shear coupling effects for the anti-symmetric case is demonstrated by the overly stiff predictions shown for UMARC* (UMARC version without shear deformation). The frequency predictions of CORBA are shown to agree very well with those of UMARC in both cases. There is a small discrepancy in the predictions of the second lag modes, but this amounts to less than 4 percent. Of greater importance is the discrepancy of both beam analyses with respect to the experimental results. The correlation of CORBA with the experimental results is shown to be poor, particularly in the lag mode, for both the symmetric and anti-symmetric cases. The error is mostly likely caused by neglecting some important warping terms in the cross section analysis.

Warping Influences on the Anti-Symmetric Box Beam

The cross section analysis employed in the verification studies of the last section considered only the out-of-plane torsion-related warping. Account of this warping effect gave a much more flexible and accurate torsional stiffness value. Analogously, the shear stiffness of the beam is also decreased by warping of the cross section. In this case, the majority of the effect is due to deformation of the cross section associated with shear forces both inplane (anticlastic deformation) and

Table 6: Rotating frequencies of the *Series 2* symmetric case at $\Omega = 1002$ RPM.

CORBA (Hz)	UMARC (Hz)	Exp. (Hz)	CORBA† Diff. (%)	Pred. Mode
36.92	36.87	35.20	4.88	1st flap
62.79	62.45	53.80	16.7	1st lag
205.0	203.0	188.0	9.04	2nd flap
392.2	378.9			2nd lag
729.9	729.2			1st tor.

† Correlation with experimental results.

out-of-plane. A simplified approach for including shear-related warping effects in a beam is to reduce the effective shear stiffness by a factor K which represents the ratio of average shear stress over the cross section to the shear stress at the centroid. This factor accounts for the near-parabolic distribution of shear stress through the cross section in the direction of the applied shear force, and is generally referred to as Timoshenko's shear correction factor. Since the amount of warping due to a shear load depends on the shape and material of the cross section, so does the value of K. The value of K was determined, using the formulas derived by Cowper (1966), as approximately 0.85 for the anti-symmetric box beam.

The influence of the shear stiffness effect on bending behavior was examined for the *Series 2* anti-symmetric box beam, but with variations of the laminate ply angles. The basic ply structure of the anti-symmetric box beam is $[\theta]_6$ on top and one side, and $[-\theta]_6$ on bottom and the other side, where $\theta = 15°$ for the baseline anti-symmetric configuration. The ply angle was varied from $\theta = 0°$ to $\theta = 45°$ for this study. The beam was considered non-rotating so as to isolate the elastic effects from the rotational effects.

For this study, the results of CORBA were compared with those of an anisotropic 3-D p-version finite element analysis developed by Hinnant (1992). The 3-D analysis used four brick elements to model the box beam. Convergence was achieved with ninth order polynomials for displacements along the length of the beam, cubic polynomials along the sides of the cross section walls, and linear polynomials through the thickness of each laminate. The material properties of each brick finite element were determined by averaging the material properties for each ply in the laminate over the laminate thickness. For cases in which the box beam was twisted, each brick element was twisted in a continuous manner such that the finite element model did not differ from the physical model by more than one hundredth of an inch at any point.

Results of the ply angle sweep for the anti-symmetric box beam, both with and without the shear correction factor applied, are illustrated in Fig. 1, shown as a function of error in the CORBA analysis with respect to the 3-D analysis. The error in the first bending modes is shown to increase rapidly with ply angle, maximizing at about $\theta = 25°$, and then decrease with ply angle. This is consistent with what might be expected based on the Poisson effects because the Poisson's ratio of the box beam laminates follows a similar trend with ply angle. The cross section warping is dependent on the Poisson's ratio, so errors associated with not including all the effects of warping are expected. The worst error is quite significant, about 16 percent in the first lag mode and about 6 percent in the first flap mode. The error in the second and third bending modes is shown to be higher, with error maximizing at about $\theta = 20°$. The shear correction factor is shown to greatly reduce these errors, giving a very accurate prediction in the flap modes.

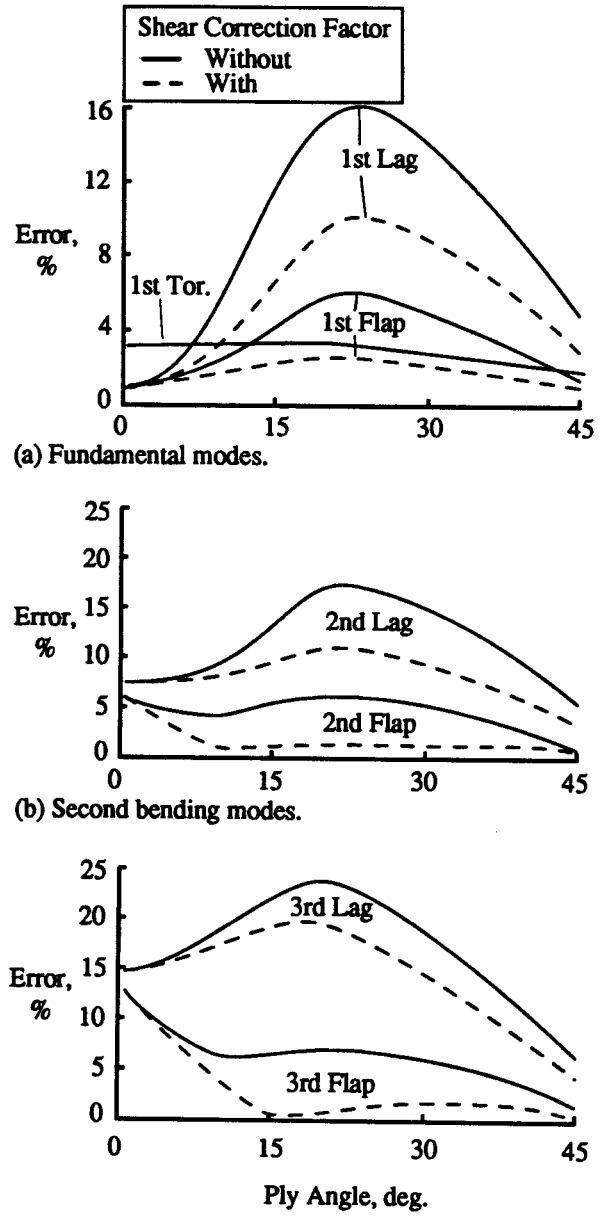

Figure 1: Error in frequency predictions as a function of ply angle for the anti-symmetric box beam.

In a second approach taken to account for all warping influences, the lag bending stiffness was determined through iteration (using the CORBA analysis) as that required to drive the first lag bending frequency to zero error. The error of the second and third lag bending modes associated with the new lag stiffness are illus-

trated in Fig. 2. As shown, the error in the higher lag bending modes is reduced, with less than five percent error at $\theta = 30°$ where previously the error was in the 10 to 25 percent range. This is an important result because it shows that even in cases where the warping effects are significant, the frequencies of higher modes may be accurately predicted if the same is true of the fundamental modes. The result is not obvious because the importance of direct shear effects increases at higher modes (beam is effectively shorter).

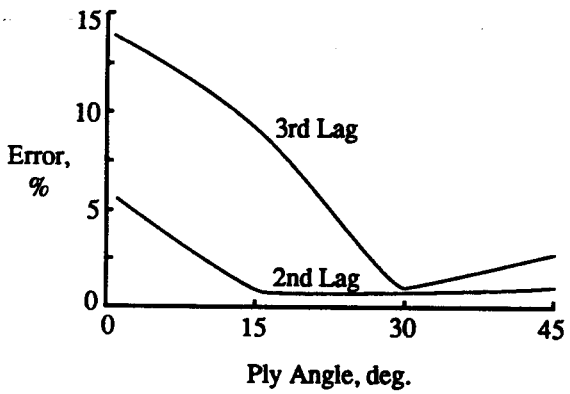

Figure 2: Error in lag mode bending frequency predictions after matching fundamental mode frequencies.

The rotating box beam with $[15]_6$ layup was then considered with the appropriate stiffness terms as developed in the nonrotating study. The results are shown in Table 7 to be greatly improved over those of Table 5, indicating that effects associated with rotation have a negligible influence on the accuracy of the frequency predictions.

Table 7: Rotating frequencies of an anti-symmetric layup box beam at $\Omega = 1002$ RPM with refined stiffness properties.

CORBA (Hz)	Experiment (Hz)	CORBA Error (%)	Pred. Mode
34.78	33.60	3.50	1st flap
47.04	46.60	0.93	1st lag
190.4	184.0	3.46	2nd flap
293.4			2nd lag
493.6			1st tor.

Warping Influences on the Symmetric Box Beam

The symmetric box beam case was also examined as a function of ply angle in the nonrotating configuration. For the symmetric box beam case, the shear is uncoupled from bending and should have little effect on the bending frequencies. The plots of Fig. 3 show that there is a dependency of the error (calculated with respect to the 3-D analysis results) on the ply orientation, just as there was for the anti-symmetric case. The error in the prediction of the fundamental torsion mode (which is coupled to the flap bending mode) is shown to increase with ply angle to a maximum at $\theta = 45°$, while the error in the lag mode (which is decoupled from torsion and flap) maximizes at about 25°. The error in

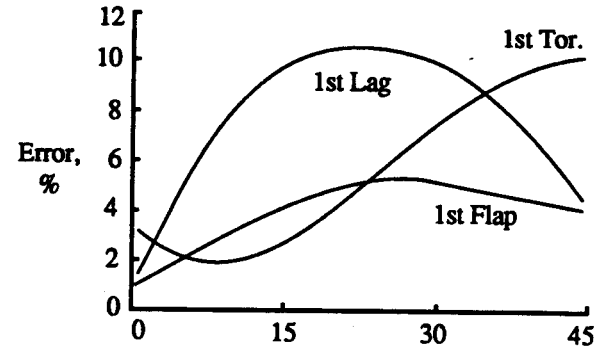

(a) Fundamental modes.

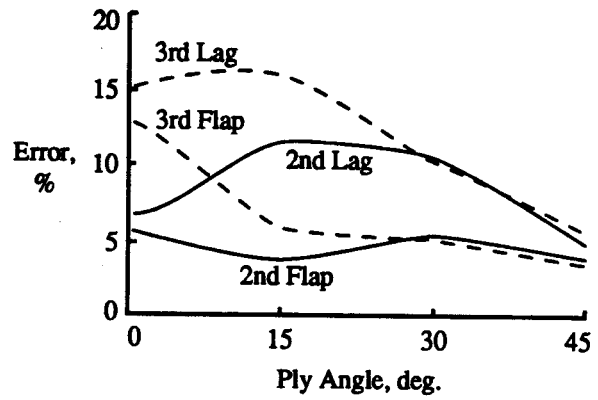

(b) Second and third bending modes.

Figure 3: Error in frequency predictions as a function of ply angle for the symmetric box beam.

the higher lag and flap modes does not follow the same path as the error in the fundamental lag mode with respect to the ply angle variations. The higher modes are shown to improve while the fundamental lag mode worsens for the ply angles above 30°.

A new torsional stiffness was determined which gave a zero error in the fundamental torsion mode. The procedure used was the same iterative procedure used previously to obtain the improved lag stiffnesses for the anti-symmetric case. It was found that the improvement to the torsional stiffness drove not only the fundamental torsion mode error to zero, but also drove the flap bending mode error to near zero because of the coupling between the two modes. The reverse was found not to be true, driving the flap bending mode to zero error did not correct the torsion mode error. Since both the fundamental torsion and flap bending modes could be corrected by adjusting a single stiffness value, the errors associated with the flap bending and torsion modes were likely from the same source, which was probably an alteration of the torsion-related warping function at the high ply angles.

An improved lag stiffness was also calculated using the iterative procedure. The error of the lag bending mode is attributed to out-of-plane warping associated with bending since this mode is decoupled from all other modes.

Application of the refined torsion and lag bending stiffnesses improved predictions of the higher bending modes as shown in Fig. 4. It is interesting that the

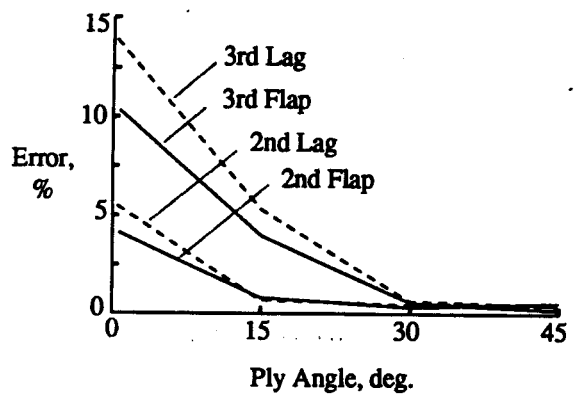

Figure 4: Error in high mode bending frequency predictions after matching fundamental mode frequencies.

error in the higher modes, after the corrections were applied, are lower at high ply angles where the beam is highly coupled and are worse at zero degrees ply angle where the beam is uncoupled.

Effects of Large Pretwist on Nonclassical Effects

Another important influence on composite blades is that of the built-in pretwist. The influence of pretwist could create problems for the approach of the present formulation because it is difficult to account for a global effect like pretwist in the local cross section analysis. The study of Shield (1982) illustrated the significant influence of pretwist on cross section deformations of bars, and the study of Kosmatka (1992) showed that pretwist has a significant influence on the cross section deformations and extension-torsion behavior of solid and thin-wall airfoil sections. The static behavior of pretwisted elastically-coupled composite beams was studied by Iesan (1976), Kosmatka and Dong (1991), and Kosmatka (1991). These studies indicate that the elastic-coupling and nonclassical influences of shear-deformation and warping can be influenced by the pretwist of the beam. There are no known reports to date, however, indicating the magnitude of the effect that the pretwist may have on the dynamic behavior of elastically-coupled beams typical of rotor blades.

The influence of the pretwist on the nonclassical effects of shear deformation and warping were examined for the nonrotating symmetric and anti-symmetric box beam cases of *Series 2* with $\theta = 15°$. The error of the CORBA predictions as compared with the 3-D results are shown in Fig. 5 for pretwist angles up to 90° in the anti-symmetric case. The change in error is small for the fundamental modes, with error change less than five percent from the untwisted case, even in the extreme case of 90° of pretwist. The error in the higher lag modes is shown to be only slightly larger, with a change in the error from 9 to about 16 percent in the third lag mode. The change in error of both the fundamental and higher modes, as a function of pretwist, was negligible for the symmetric case.

Convergence Study

A convergence study was performed to determine if use of higher order elements is beneficial when beams are elastically coupled. A standard h-element is defined for purposes of the present discussion as one with cubic

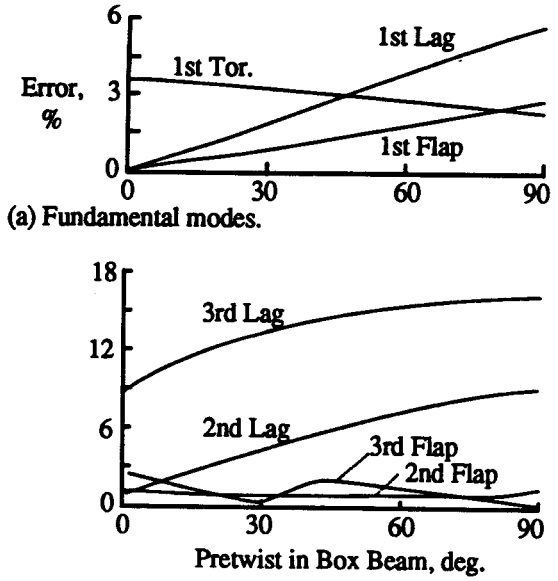

Figure 5: Error in frequency predictions as a function of the anti-symmetric beam pretwist.

bending shape functions and quadratic axial and torsion displacement approximations. The equivalent p-version element of the present formulation has $p_u = 1$ and $p_\phi = 1$. Since this element is common in rotor analysis, the convergence study will consider it a baseline for comparison. Elements with higher order than the standard are referenced by their addition to the displacement approximations. For example, "Std.+1w+1t" refers to a beam element with one order higher approximation in flap bending and torsion than the standard element.

A convergence study of a bending-twist-coupled untwisted composite box beam showed slow convergence of the third predominantly flap mode. The cause of this was probably due to the coupling between the bending and torsion modes. Various shape function approximation schemes were employed to determine an optimum for convergence of this particular mode. The results are illustrated in the plot of Fig. 6 which shows that the "Std.+1w+1t" approximation scheme had the best convergence. Use of that approximation scheme decreased the total number of degrees of freedom from 32 to 22, assuming a 1 percent error criteria. This amounts to about a one-third reduction in global degrees of freedom which could relate to significant improvements in run times associated with analyses of elastically-coupled blades.

The composite box beam considered in the above study was uniform and untwisted. A second study was conducted on the same beam with 40° of pretwist. In this case, the cross section properties change as a function of x, and, as a result, the integrations were not exact. Again, various shape function approximation schemes were employed to determine an optimum for convergence of the third flapwise bending mode. The results are illustrated in the plot of Fig. 7 which shows that there is no optimum. The convergence rates are also much shallower than those shown for the untwisted case in Fig. 6. This is because in addition to the elastic

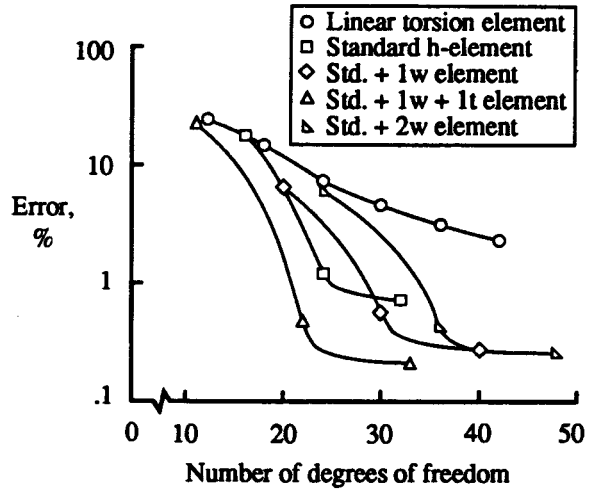

Figure 6: Convergence of the untwisted symmetric-case box beam.

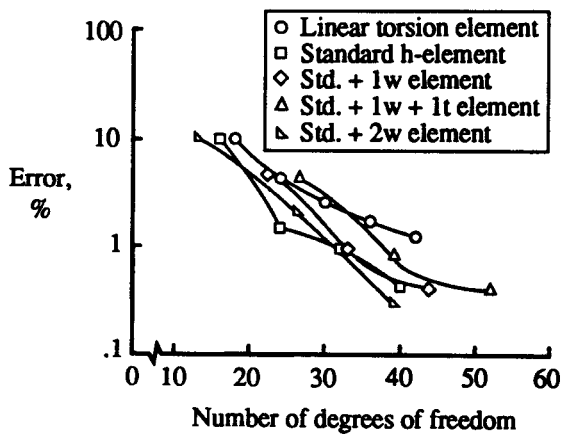

Figure 7: Convergence of the 40° twisted symmetric-case box beam.

coupling between flap and torsion modes, the pretwist introduces coupling between the bending modes. The only higher-order element which performed well had additonal order increases in both bending modes as well as torsion. However, for this twisted case, the higher order elements did nothing to improve efficiency, and in some cases even degraded it.

CONCLUSIONS

A dynamic analysis has been formulated for rotating pretwisted composite blades which exhibit anisotropic behavior. The present formulation incorporated the effects of shear deformation implicitly through elimination of the shear variables in the material compliance matrix. Results showed that this approach was able to capture the most significant effect of shear deformation, namely the reduction in effective bending stiffness that occurs when a substantial amount of bending-shear coupling is present in a beam. The difference between implicit and explicit use of shear degrees of freedom was shown to be less than 2 percent up to the second bending modes of some representative rotor blades, and less than 4 percent up to the second bending modes of some highly coupled box beam specimens.

The results of this study also showed that one-dimensional global dynamic analysis based on classical beam kinematics can accurately predict the bending and torsion frequencies of modes important to an aeroelastic analysis. However, the section properties used in the global analysis must account for the important nonclassical effects associated with shear deformation, warping, and elastic couplings. These nonclassical effects were shown to have significant influence on the frequencies of the fundamental modes of highly coupled beam structures. Errors on the order of fifteen percent were reduced to less than five percent through account of the nonclassical effects. The influence of twist on the predictive capabilities of the analysis was shown to be small.

The present analysis (CORBA) was implemented using a p-version beam finite element. Both the advantages and disadvantages of this approach were discussed. The p-version element proved to be convenient for assuring a converged solution, and allowed the desired flexibility in tailoring the displacement approximations to the dynamic characteristics of a given beam configuration. Some degree of efficiency improvement was demonstrated for the uniform untwisted case, but efficiency does not appear to be an issue for more realistic rotor blade structures. Much of the efficiency of using higher order elements was shown to be lost for a highly twisted blade.

REFERENCES

Chandra, R., and Chopra, I., 1989, "Experimental Theoretical Investigation of the Vibration Characteristics of Rotating Composite Box-Beams," *Presented at the American Helicopter Society National Technical Specialists' Meeting on Rotorcraft Dynamics*, Arlington, Tx.

Cowper, G.R., 1966, "The Shear Coefficient in Timoshenko's Beam Theory," *Journal of Applied Mechanics*, June, pp. 335-340.

Hinnant, H.E., 1989, "Derivation of a Tapered p-Version Beam Finite Element," NASA TP 2931.

Hinnant, H.E., 1992, "A Curvilinear, Anisotropic, p-Version, Brick Finite Element Based on Geometric Entities," *Proceedings of the 33rd Structures, Structural Dynamics, and Materials Conference*, Dallas, Tx, AIAA Paper No. 92-2329.

Hodges, D.H. and Atilgan, A.R., 1991, "Asymptotical Modeling of Initially Curved and Twisted Composite Rotor Blades," *Proceedings of the AHS International Technical Specialists' Meeting on Rotorcraft Basic Research*, Atlanta, Georgia, March 25-27.

Hodges, D.H., Hopkins, A.S., Kunz, D.L., and Hinnant, H.E., 1990, "General Rotorcraft Aeromechanical Stability Program (GRASP) Theory Manual," NASA TM 102255.

Hodges, R.V., Nixon, M.W., and Rehfield, L.W., 1987, "Comparison of Composite Rotor Blade Models: A Coupled-Beam Analysis and an MSC/NASTRAN Finite-Element Model," NASA TM 89024.

Hong, C.H. and Chopra, I., 1985a, "Aeroelastic Stability Analysis of a Composite Rotor Blade," *Journal of the American Helicopter Society*, Vol. 30, No. 2, pp.57-67.

Hong, C.H. and Chopra, I., 1985b, "Aeroelastic Stability Analysis of a Composite Bearingless Rotor Blade," *Journal of the American Helicopter Society*, Vol. 31, No. 4, pp. 29-35.

Iesan, D., 1976, "Saint-Venant's Problem for Inhomogeneous and Anisotropic Elastic Bodies," *Journal of Elasticity*, Vol. 6, pp. 277-294.

Kaza, K.R., and Kvaternik, R.G., 1977, "Nonlinear Aeroelastic Equations for Combined Flapwise Bending, Chordwise Bending, Torsion, and Extension of Twisted, Nonuniform Rotor Blades in Forward Flight," NASA TM 74059.

Kosmatka, J.B., 1986, "Structural Dynamic Modeling of Advanced Composite Propellers by the Finite Element Method," Ph.D. Dissertation, University of California, Los Angeles.

Kosmatka, J.B., 1988, "Analysis of Composite Rotor Blades Via Saint Venant's Elasticity Solutions," *Presented at the 14th European Rotorcraft Forum*, Milano, Italy.

Kosmatka, J.B., 1991, "Extension-Bend-Twist Coupling Behavior of Thin-Walled Advanced Composite Beams with Initial Twist," *Proceedings of the 32nd Structures, Structural Dynamics, and Materials Conference*, Baltimore, MD, AIAA Paper No. 91- 1023-CP, Vol. 2, pp. 1037-1049.

Kosmatka, J.B., 1992, "On the Behavior of Pretwisted Beams with Irregular Cross Sections," *ASME Journal of Applied Mechanics*, Vol. 59, pp. 146-152.

Kosmatka, J.B. and Dong, S. B., 1991, "Saint-Venant Solutions for Prismatic Anisotropic Beams," *International Journal of Solids and Structures*, Vol. 28, No. 7, pp. 917-938.

Kosmatka, J.B., and Ie, C., 1991, "On the Vibration Behavior of Shear-Deformable Prismatic Beams Including In-Plane Cross-Section Deformations," *Proceedings of the 32nd Structures, Structural Dynamics, and Materials Conference*, Baltimore, MD, AIAA Paper No. 91-1201-CP, Vol. 2, pp. 1462-1474.

Nixon, M.W., 1989, "Analytical and Experimental Investigations of Extension-Twist-Coupled Structures," George Washington University Masters Thesis, Hampton, VA.

Rehfield, L.W., Atilgan, A.R., and Hodges, D.H., 1990, "Non-Classical Behavior of Thin-Walled Composite Beams With Closed Cross Sections," *Journal of the American Helicopter Society*, Vol. 35, (2).

Shield, R. T., 1982, "Extension and Torsion of Elastic Bars with Initial Twist," *ASME Journal of Applied Mechanics*, Vol. 49, pp. 779-786.

Smith, E.C. and Chopra, I., 1990, "Formulation and Evaluation of an Analytical Model for Composite Box-Beams," *Journal of the American Helicopter Society*, Vol. 36, No. 3, pp. 22-35.

Smith, E.C., and Chopra, I.C., 1992, "Aeroelastic Response and Blade Loads of a Composite Rotor in Forward Flight," *Proceedings of the 33rd Structures, Structural Dynamics, and Materials Conference*, Dallas, Tx, AIAA Paper No. 92-2566.

Wempner, G., 1981, *Mechanics of Solids with Applications to Thin Bodies*, 1st edition, McGraw-Hill Book Co., New York, N.Y.

APPENDIX A
STRAIN AND KINETIC ENERGY FORMULATION

As the formulation presented here is nonlinear and explicit, the number of terms in the energy expressions can quickly grow to an unmanageable size. Further, many of the terms may be negligible compared to other important terms. To reduce the number of terms to only those of significance, an ordering scheme is employed where terms of $O(\epsilon^{n+2})$ and higher are eliminated in the presence of terms of $O(\epsilon^n)$. All displacement variables defined in this formulation are assigned an order of ϵ with two exceptions. The axial displacement u_e is of order ϵ^2 and the twist deformation ϕ is of order one. The latter exception results from making the analysis accurate for rotor blades with very large elastic couplings associated with twist deformation.

Geometry and Coordinates

The present formulation requires six coordinate systems. *Shaft*, *gimballed*, and *hub-fixed* coordinate systems are defined as illustrated in Fig. 8. For purposes of

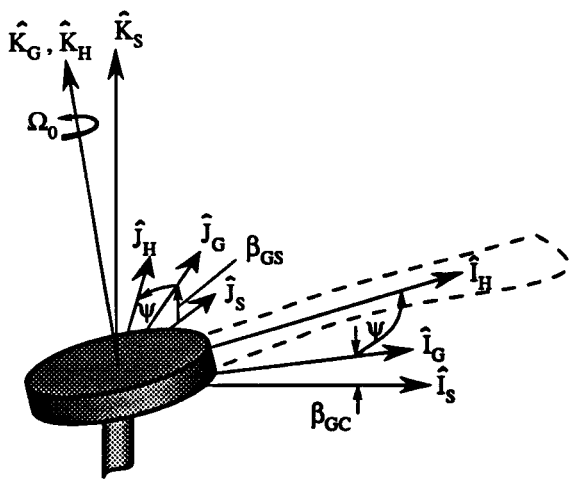

Figure 8: Geometry of the shaft, gimbal and hub.

the present formulation, the shaft reference frame is an inertial system. A *blade* reference frame $(\hat{e}_x, \hat{e}_y, \hat{e}_z)$ is defined with its x-axis directed along the elastic axis of the undeformed blade as shown in Fig. 9. The elastic part of the blade is offset from the center of rotation a distance $h_x\hat{e}_x$. A *cross-section* reference frame $(\hat{e}_x, \hat{e}_\eta, \hat{e}_\zeta)$ is defined with origin at some position $(h_x + x)\hat{e}_x$ along the elastic axis of the blade, and with origin on that axis acting as the reference point for the cross section. The unit vector $\hat{e}_\eta$ is directed along the chord direction of the blade cross section while $\hat{e}_\zeta$ is defined by the cross product of $\hat{e}_x$ and $\hat{e}_\eta$. Thus, the cross-section system is an orthonormal vector set which rotates with the built-in pretwist of the undeformed blade. A *deformed* reference frame $(\hat{E}_x, \hat{E}_\eta, \hat{E}_\zeta)$ is identical to the cross-section set before deformation, but translates and rotates with the bending and twist of the rigid cross section plane to a new position after deformation.

The unit vector triads of each coordinate system are related by the following equations:

$$\begin{Bmatrix} \hat{I}_G \\ \hat{J}_G \\ \hat{K}_G \end{Bmatrix} = [T_{GS}] \begin{Bmatrix} \hat{I}_S \\ \hat{J}_S \\ \hat{K}_S \end{Bmatrix} \tag{10}$$

$$\begin{Bmatrix} \hat{I}_H \\ \hat{J}_H \\ \hat{K}_H \end{Bmatrix} = [T_{HG}] \begin{Bmatrix} \hat{I}_G \\ \hat{J}_G \\ \hat{K}_G \end{Bmatrix} \tag{11}$$

$$\begin{Bmatrix} \hat{e}_x \\ \hat{e}_y \\ \hat{e}_z \end{Bmatrix} = [T_{BH}] \begin{Bmatrix} \hat{I}_H \\ \hat{J}_H \\ \hat{K}_H \end{Bmatrix} \tag{12}$$

$$\begin{Bmatrix} \hat{e}_x \\ \hat{e}_\eta \\ \hat{e}_\zeta \end{Bmatrix} = [T_{CB}] \begin{Bmatrix} \hat{e}_x \\ \hat{e}_y \\ \hat{e}_z \end{Bmatrix} \tag{13}$$

$$\begin{Bmatrix} \hat{E}_x \\ \hat{E}_\eta \\ \hat{E}_\zeta \end{Bmatrix} = [T_{DC}] \begin{Bmatrix} \hat{e}_x \\ \hat{e}_\eta \\ \hat{e}_\zeta \end{Bmatrix} \tag{14}$$

and the transformations matrices are themselves given by:

$$[T_{GS}] = \begin{bmatrix} \cos\beta_{GC} & 0 & -sin\beta_{GC} \\ 0 & 1 & 0 \\ \sin\beta_{GC} & 0 & \cos\beta_{GC} \end{bmatrix} \begin{bmatrix} 1 & 0 & 0 \\ 0 & \cos\beta_{GS} & \sin\beta_{GS} \\ 0 & -\sin\beta_{GS} & \cos\beta_{GS} \end{bmatrix} \tag{15}$$

$$[T_{HG}] = \begin{bmatrix} \cos\psi & \sin\psi & 0 \\ -\sin\psi & \cos\psi & 0 \\ 0 & 0 & 1 \end{bmatrix} \tag{16}$$

$$[T_{BH}] = \begin{bmatrix} \cos\beta_P & 0 & -sin\beta_P \\ 0 & 1 & 0 \\ \sin\beta_P & 0 & \cos\beta_P \end{bmatrix} \tag{17}$$

$$[T_{CB}] = \begin{bmatrix} 1 & 0 & 0 \\ 0 & \cos\beta & \sin\beta \\ 0 & -\sin\beta & \cos\beta \end{bmatrix} \tag{18}$$

The transformation between the deformed and cross-section systems $[T_{DC}]$ is derived later in this appendix.

Strain Energy Derivation

Consider the position of a point on the cross section of a rotor blade before deformation with position vector given by

$$\vec{r}_0 = (h_x + x)\hat{e}_x + \eta\hat{e}_\eta + \zeta\hat{e}_\zeta \tag{19}$$

After deformation, the position vector is given by

$$\vec{R} = \vec{R}_0 + \vec{R}_E + \vec{R}_W \tag{20}$$

where $\vec{R}_0$ represents deformed position of the cross section reference point, $\vec{R}_E$ represents deformation associated with the rigid rotation of the cross section, and $\vec{R}_W$ represents deformation associated with warping of the cross section. The position vectors are defined as follows:

$$\vec{R}_0 = (h_x + x + u_0)\hat{e}_x + v_0\hat{e}_\eta + w_0\hat{e}_\zeta \tag{21}$$

$$\vec{R}_E = 0\hat{E}_x + \eta\hat{E}_\eta + \zeta\hat{E}_\zeta \tag{22}$$

$$\vec{R}_W = W_u\hat{E}_x + W_\eta\hat{E}_\eta + W_\zeta\hat{E}_\zeta \tag{23}$$

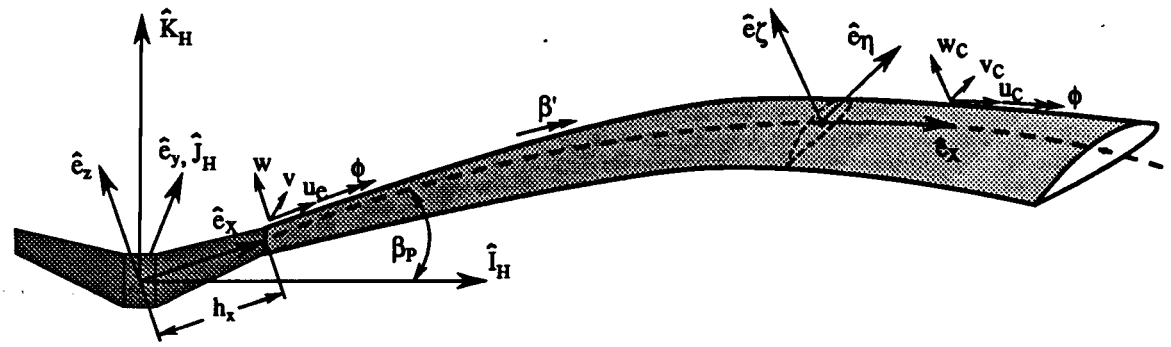

Figure 9: Geometry of the elastic blade.

where W_u, W_η, and W_ζ are warping displacements defined as

$$W_u = u'\psi_{uA} + w'_{c_s}\psi_{uQ_\zeta} + \theta_\eta\psi_{uM_\eta} + v'_{c_s}\psi_{uQ_\eta} + \theta_\zeta\psi_{uM_\zeta} + \phi'\psi_{uT} \quad (24)$$

$$W_\eta = u'\psi_{\eta A} + w'_{c_s}\psi_{\eta Q_\zeta} + \theta_\eta\psi_{\eta M_\eta} + v'_{c_s}\psi_{\eta Q_\eta} + \theta_\zeta\psi_{\eta M_\zeta} + \phi'\psi_{\eta T} \quad (25)$$

$$W_\zeta = u'\psi_{\zeta A} + w'_{c_s}\psi_{\zeta Q_\zeta} + \theta_\eta\psi_{\zeta M_\eta} + v'_{c_s}\psi_{\zeta Q_\eta} + \theta_\zeta\psi_{\zeta M_\zeta} + \phi'\psi_{\zeta T} \quad (26)$$

where subscript s denotes shear strains due to shear deformation and θ is rotation due to bending. The warping terms represent nonclassical contributions to the displacements as a result of cross section deformation. The notation for the warping ψ_{ij} gives the displacement in the direction i associated with a load j, and the magnitude of the displacement in the i direction is shown to be proportional to the displacement associated with the load direction. The displacements associated with warping are in general small for beam structures, with only a few exceptions. The most well-known exception is the out-of-plane warping associated with torsion of noncircular beams (ψ_{uT} in the present formulation). With a completely general approach to anisotropic beam theory, any of the 18 warping terms shown above could be significant for a particular configuration. Thus, for the general approach, all of the warping terms would be maintained within the ordering scheme, even though for most practical cases all but a few terms could be eliminated.

However, the warping displacements have little use in a one-dimensional analysis because the primary objective is accurate assessment of global behavior. The important contribution of warping has been shown in past studies to be a reduction in the effective beam stiffnesses. As such, the warping unnecessarily complicates development of the one-dimensional analysis and will be eliminated except for some key terms which have been shown to be important, even for isotropic beams. The other effects of warping can be captured in a detailed cross section (local) analysis which is uncoupled from the beam (global) analysis.

The warping terms which are retained are the out-of-plane torsion-related warping ψ_{uT}, and the two out-of-plane shear-related warping terms ψ_{uQ_ζ} and ψ_{uQ_η}. If the Timoshenko-type shear deformation model is applied (the cross section is assumed to remain plane), then $\psi_{uQ_\zeta} = \zeta$ and $\psi_{uQ_\eta} = \eta$. The deformed position vector is then rewritten with $\vec{R}_w = [\phi'\psi_{uT} + v'_{c_s}\eta + w'_{c_s}\zeta]\hat{E}_x$ as

$$\vec{R} = (\{h_x + x + u_0, v_0, w_0\} + \{(\phi'\psi_{uT} + v'_{c_s}\eta + w'_{c_s}\zeta), \eta, \zeta\}[T_{DC}]) \begin{Bmatrix} \hat{e}_x \\ \hat{e}_\eta \\ \hat{e}_\zeta \end{Bmatrix} \quad (27)$$

where T_{DC} is the transformation matrix between the deformed and cross-section coordinate systems, and will be derived in the next paragraph.

The sequence of rotations for transformation from the undeformed cross-section axis system to the deformed axis system is $\{\theta_\zeta, -\theta_\eta, \phi\}$ where θ_ζ is the Euler bending rotation in the lead-lag plane (given no pretwist), θ_η is the Euler bending rotation in the flapwise plane (given no pretwist), and ϕ is the elastic twist which may be a large angle. The transformation matrix is then defined as

$$[T_{DC}] = \begin{bmatrix} 1 & 0 & 0 \\ 0 & \cos\phi & \sin\phi \\ 0 & -\sin\phi & \cos\phi \end{bmatrix} \begin{bmatrix} 1 & 0 & -\theta_\eta \\ 0 & 1 & 0 \\ \theta_\eta & 0 & 1 \end{bmatrix} \begin{bmatrix} 1 & \theta_\zeta & 0 \\ -\theta_\zeta & 1 & 0 \\ 0 & 0 & 1 \end{bmatrix} \quad (28)$$

where the small angle assumption has been employed for the bending rotations. The rotations may be written in terms of the cross-section kinematic variables as

$$\theta_\zeta = (v_{c,x} - \beta_{,x}w_c)\hat{e}_\eta \quad (29)$$

$$-\theta_\eta = (w_{c,x} + \beta_{,x}v_c)\hat{e}_\zeta \quad (30)$$

which, when substituted into Eqn. 28, gives the transformation matrix as

$$[T_{DC}] = \begin{bmatrix} 1 & v'_c - w_c\beta' & w'_c + v_c\beta' \\ -(v'_c - w_c\beta')\cos\phi + (w'_c + v_c\beta')\sin\phi & \beta_c\sin\phi + \cos\phi & \sin\phi \\ -(w'_c + v_c\beta')\cos\phi + (v'_c - w_c\beta')\sin\phi & \beta_c\cos\phi - \sin\phi & \cos\phi \end{bmatrix} \quad (31)$$

where,

$$\beta_c = -(v_c' - w_c\beta')(w_c' + v_c\beta') \tag{32}$$

This transformation agrees with that of Kosmatka (1986) if ϕ is assumed to be a small angle.

The strains are developed in terms of the displacements by substituting the derivatives of the position vectors into the strain component definitions as given in Wempner (1981). The position vectors have been defined in terms of the cross-section coordinates, and the derivatives were calculated as follows:

$$\begin{aligned}
\vec{r}_{,x} &= \{1,0,0\} && (33)\\
\vec{r}_{,\eta} &= \{0,1,0\} && (34)\\
\vec{r}_{,\zeta} &= \{0,0,1\} && (35)\\
\vec{R}_{,x} &= \{G_{x1}, G_{x2}, G_{x3}\} && (36)\\
\vec{R}_{,\eta} &= \{G_{\eta 1}, G_{\eta 2}, G_{\eta 3}\} && (37)\\
\vec{R}_{,\zeta} &= \{G_{\zeta 1}, G_{\zeta 2}, G_{\zeta 3}\} && (38)
\end{aligned}$$

where the G_i terms are defined within the ordering scheme as:

$$\begin{aligned}
G_{x1} =& \\
& 1 + u_c' - \eta\kappa_\eta - \zeta\kappa_\zeta + \\
& \phi' \left[(\zeta v_c' + \eta w_c' - \eta v_c\beta' - \zeta w_c\beta')\cos\phi \right.\\
& \left. + (\eta v_c' + \zeta w_c' + \zeta v_c\beta' - \eta w_c\beta')\sin\phi\right] \\
& +(\phi'\psi_{uT})' && (39)\\
G_{x2} =& \\
& v_c' - w_c\beta' - \phi'[\zeta\cos\phi + \eta\sin\phi] && (40)\\
G_{x3} =& \\
& w_c' + v_c\beta' + \phi'[\eta\cos\phi - \zeta\sin\phi] && (41)\\
G_{\eta 1} =& \\
& v_{c_s}' - (v_c' - w_c\beta')\cos\phi - (w_c' + v_c\beta')\sin\phi + \\
& \phi'\psi_{uT,\eta} && (42)\\
G_{\eta 2} =& \\
& \cos\phi + (v_c w_c \beta'^2 - v_c v_c'\beta' + \\
& w_c w_c'\beta' - v_c' w_c')\sin\phi && (43)\\
G_{\eta 3} =& \\
& \sin\phi && (44)\\
G_{\zeta 1} =& \\
& w_{c_s}' - (w_c' + v_c\beta')\cos\phi + (v_c' - w_c\beta')\sin\phi + \\
& \phi'\psi_{uT,\zeta} && (45)\\
G_{\zeta 2} =& \\
& -\sin\phi + (v_c w_c \beta'^2 - v_c v_c'\beta' + \\
& w_c w_c'\beta' - v_c' w_c')\cos\phi && (46)\\
G_{\zeta 3} =& \\
& \cos\phi && (47)
\end{aligned}$$

and the curvatures are given by

$$\begin{aligned}
\kappa_\eta &= (v_c'' - w_c\beta'' - 2w_c'\beta' - v_c\beta'^2)\cos\phi + \\
&\quad (w_c'' + v_c\beta'' + 2v_c'\beta' - w_c\beta'^2)\sin\phi && (48)\\
\kappa_\zeta &= (w_c'' + v_c\beta'' + 2v_c'\beta' - w_c\beta'^2)\cos\phi - \\
&\quad (v_c'' - w_c\beta'' - 2w_c'\beta' - v_c\beta'^2)\sin\phi && (49)
\end{aligned}$$

and κ_η is the curvature in the flapwise plane and κ_ζ is curvature in the lead-lag plane. The strain component definitions simplify after substitution of the undeformed position vectors to

$$\begin{aligned}
\epsilon_{xx} &= (\hat{R}_{,x}\cdot\hat{R}_{,x} - 1)/2 && (50)\\
\epsilon_{x\eta} &= (\hat{R}_{,x}\cdot\hat{R}_{,\eta}) && (51)\\
\epsilon_{x\zeta} &= (\hat{R}_{,x}\cdot\hat{R}_{,\zeta}) && (52)\\
\epsilon_{\eta\eta} &\approx \epsilon_{\zeta\zeta} \approx \epsilon_{\eta\zeta} \approx 0 && (53)
\end{aligned}$$

where $\epsilon_{x\eta}$ and $\epsilon_{x\zeta}$ are the engineering form of the shear strains. The three nonzero strains are calculated by carrying out the dot products. In terms of the displacements defined in the cross-section system, these are shown after application of the ordering scheme.

$$\begin{aligned}
\epsilon_{xx} &= u_c' + \frac{1}{2}(v_c' - w_c\beta')^2 + \frac{1}{2}(w_c' + v_c\beta')^2 - \\
&\quad \eta\kappa_\eta - \zeta\kappa_\zeta + \frac{1}{2}(\eta^2 + \zeta^2)\phi'^2 + (\phi'\psi_{uT})' && (54)\\
\epsilon_{x\eta} &= v_{c_s}' + (\psi_{uT,\eta} - \zeta)\phi' && (55)\\
\epsilon_{x\zeta} &= w_{c_s}' + (\psi_{uT,\zeta} + \eta)\phi' && (56)
\end{aligned}$$

These strains are defined in terms of the blade coordinate system through use of the transformation $[T_{CB}]$ as

$$\begin{aligned}
\epsilon_{xx} &= u' + \frac{1}{2}v'^2 + \frac{1}{2}w'^2 + \frac{1}{2}(\eta^2 + \zeta^2)\phi'^2 \\
&\quad -v''[\eta\cos(\beta+\phi) - \zeta\sin(\beta+\phi)] \\
&\quad -w''[\eta\sin(\beta+\phi) + \zeta\sin(\beta+\phi)] \\
&\quad +(\phi'\psi_{uT})' && (57)\\
\epsilon_{x\eta} &= v_s'\cos(\beta+\phi) + w_s'\sin(\beta+\phi) + \\
&\quad (\psi_{uT,\eta} - \zeta)\phi' && (58)\\
\epsilon_{x\zeta} &= w_s'\cos(\beta+\phi) - v_s'\sin(\beta+\phi) + \\
&\quad (\psi_{uT,\zeta} + \eta)\phi' && (59)
\end{aligned}$$

At this point a variable substitution is made which eliminates the kinematic contribution of forshortening from the axial displacement. It has been shown by Kaza and Kvaternik (1977) that this substitution provides the convenience of developing centrifugal stiffening terms associated with forshortening in the kinetic energy formulation rather than the strain energy formulation. The substitution is

$$u_e' = u' - \frac{1}{2}v'^2 - \frac{1}{2}w'^2 \tag{60}$$

where u_e' represents the elastic axial strain without kinematic contributions from transverse bending displacements. The strain components then become in final form:

$$\begin{aligned}
\epsilon_{xx} &= u_e' + \frac{1}{2}(\eta^2 + \zeta^2)\phi'^2 + (\phi'\psi_{uT})' \\
&\quad -v''[\eta\cos(\beta+\phi) - \zeta\sin(\beta+\phi)] \\
&\quad -w''[\eta\sin(\beta+\phi) + \zeta\sin(\beta+\phi)] && (61)\\
\epsilon_{x\eta} &= v_s'\cos(\beta+\phi) + w_s'\sin(\beta+\phi) + \\
&\quad (\psi_{uT,\eta} - \zeta)\phi' && (62)\\
\epsilon_{x\zeta} &= w_s'\cos(\beta+\phi) - v_s'\sin(\beta+\phi) + \\
&\quad (\psi_{uT,\zeta} + \eta)\phi' && (63)
\end{aligned}$$

The elastic stress-strain relationships employed in this formulation are given as

$$\left\{ \begin{array}{c} \sigma_{xx} \\ \sigma_{x\zeta} \\ \sigma_{x\eta} \end{array} \right\} = \left\{ \begin{array}{ccc} Q'_{11} & Q'_{15} & Q'_{16} \\ Q'_{15} & Q'_{55} & Q'_{56} \\ Q'_{16} & Q'_{56} & Q'_{66} \end{array} \right\} \left\{ \begin{array}{c} \epsilon_{xx} \\ \epsilon_{x\zeta} \\ \epsilon_{x\eta} \end{array} \right\} \quad (64)$$

where the Q'_{ij} represent the material stiffness at a loction in the cross section. The material stiffnesses are an average value based on the individual ply material and orientation, and also depend on the orientation of the laminate with respect to the cross section axes. The variation of the elastic strain energy can then be written as

$$\delta U = \int_0^R \iint_A \{\sigma_{xx}\delta\epsilon_{xx} + \sigma_{x\eta}\delta\epsilon_{x\eta} + \sigma_{x\zeta}\delta\epsilon_{x\zeta}\}\, d\eta d\zeta dx \quad (65)$$

The stress-strain relations are substituted into the strain energy variational, followed by a second substitution of the strain-displacement relations (Eqns. 61-63) for the strains. After integrating over the area, the strain energy variation becomes

$$\delta U = \int_0^R \delta\hat{v}_i \mathrm{k}_{ij} \hat{v}_j \, dx + \int_0^R \delta\hat{v}_i D_i \, dx \quad (66)$$

where $(i, j = 1, 9)$, and

$$\delta\hat{v}_i = \{ \ \delta u'_e \ \ \delta v'_s \ \ \delta w'_s \ \ \delta\phi \ \ \delta\phi' \ \ \delta w' \ \ \delta w'' \ \ \delta v' \ \ \delta v'' \ \} \quad (67)$$

The first integral of Eqn. 66 represents the linear part of the strain energy and the second term represents the nonlinear contribution to the strain energy.

Kinetic Energy Derivation

Now, the kinetic energy is derived. The position of a point on the deformed blade as given by Eqn. 27 may be written using the blade reference displacements and neglecting the warping displacements as

$$\vec{R} = (\{h_x + x + u, v, w\} + \{o, \eta, \zeta\}[T_{DB}]) \left\{ \begin{array}{c} \hat{e}_x \\ \hat{e}_y \\ \hat{e}_z \end{array} \right\} \quad (68)$$

where $[T_{DB}]$ is the transformation between the deformed and blade coordinate systems which is given by

$$[T_{DB}] = [T_{DC}][T_{CB}] \quad (69)$$

The velocity of a point on the deformed blade is written as

$$\vec{V} = \frac{\partial \vec{R}}{\partial t} + \vec{\Omega} \times \vec{R} \quad (70)$$

where

$$\begin{aligned} \vec{\Omega} &= \{\Omega_x, \Omega_y, \Omega_z\} \left\{ \begin{array}{c} \hat{e}_x \\ \hat{e}_y \\ \hat{e}_z \end{array} \right\} \\ &= \{0, 0, \Omega_0\}[T_{HG}]^T [T_{BH}]^T \left\{ \begin{array}{c} \hat{e}_x \\ \hat{e}_y \\ \hat{e}_z \end{array} \right\} \end{aligned} \quad (71)$$

and Ω_0 is the rotation rate at which the hub spins about the gimballed z_G axis. If there is no precone then $\Omega_x = \Omega_y = 0$. After application of the ordering scheme, the velocity is given by

$$\vec{V} = \{V_x, V_y, V_z\} \left\{ \begin{array}{c} \hat{e}_x \\ \hat{e}_y \\ \hat{e}_z \end{array} \right\} \quad (72)$$

$$\begin{aligned} V_x = & \\ & \dot{u} + w\Omega_y - v\Omega_z - (\Omega_z + \dot{v}')\eta\cos\beta_2 + \\ & (\Omega_y - \dot{w}')\zeta\cos\beta_2 + \eta\Omega_y\sin\beta_2 + \Omega_x\zeta\sin\beta_2 + \\ & \zeta\cos\beta_2 v'\dot{\phi} + \eta\sin\beta_2 v'\dot{\phi} - \eta\cos\beta_2 w'\dot{\phi} - \\ & \zeta\sin\beta_2 w'\dot{\phi} + \eta\sin\beta_2\dot{w}' + \zeta\sin\beta_2\dot{v}' \end{aligned} \quad (73)$$

$$\begin{aligned} V_y = & \\ & \dot{v} - w\Omega_x + (h_x + x + u)\Omega_z - \Omega_z\eta v'\cos\beta_2 - \\ & \Omega_x\zeta\cos\beta_2 - \zeta\dot{\phi}\cos\beta_2 - \Omega_z\zeta w'\cos\beta_2 - \\ & \Omega_x\eta\sin\beta_2 - \eta\dot{\phi}\sin\beta_2 - \Omega_z\eta w'\sin\beta_2 + \\ & \Omega_z\zeta v'\sin\beta_2 \end{aligned} \quad (74)$$

$$\begin{aligned} V_z = & \\ & \dot{w} + v\Omega_x - (h_x + x + u)\Omega_y + \Omega_x\eta\cos\beta_2 + \\ & \Omega_y\eta v'\cos\beta_2 + \eta\dot{\phi}\cos\beta_2 + \Omega_y\zeta v'\cos\beta_2 + \\ & \Omega_y\eta w'\sin\beta_2 - \zeta\dot{\phi}\sin\beta_2 - \Omega_x\zeta\sin\beta_2 - \\ & \Omega_y\zeta v'\sin\beta_2 \end{aligned} \quad (75)$$

where $\beta_2 = \beta + \phi$. After taking the variation of the velocity, the following substitutions, which are based on Eqn. 60, are made into $\vec{V}$ and $\delta\vec{V}$.

$$\dot{u} = \dot{u}_e - \int_0^x (v'\dot{v}' + w'\dot{w}')\, dx \quad (76)$$

$$\delta u = \delta u_e - \int_0^x (v'\delta v' - w'\delta w')\, dx \quad (77)$$

The variation of the blade kinetic energy is given by

$$\delta T = \int_0^R \iint_A \rho\vec{V} \cdot \delta\vec{V}\, d\eta d\zeta\, dx \quad (78)$$

where ρ is the mass density of the blade. After substituting the velocity as defined in Eqn. 72 into the kinetic energy expression, calculating the velocity variation, and carrying out the dot product, the variation of the kinetic energy may be written as

$$\int_0^R m\{[T_u]_i\, \delta\hat{u}_i + [T_{\dot{u}}]_i\, \delta\hat{\dot{u}}_i + T_a\, \delta\hat{u}_2 + T_F\}\, dx \quad (79)$$

where $(i = 1, 6)$ and the vector of displacement variations for the kinetic energy formulation is given by,

$$\delta\hat{u}_i = \{ \ \delta u_e \ \ \delta v \ \ \delta v' \ \ \delta w \ \ \delta w' \ \ \delta\phi \ \} \quad (80)$$

The quantities $[T_u]_i$ and $[T_{\dot{u}}]_j$ represent groups of terms which may be functions of both u and $\dot{u}$. The terms T_a and T_F represent additional terms in the kinetic energy which result from the variable substitutions defined in Eqns. 76 and 77. T_a represents the nonlinear anti-symmetric contribution of Coriolis force and is defined as

$$T_a = 2\int_0^x (v'\dot{v}' + w'\dot{w}')\, d\xi \quad (81)$$

The term T_F gives the contribution from the integral part of the variation substitution for δu_e,

$$T_F = -(x + 2\dot{v}) \int_0^x (v'\delta v' + w'\delta w')\, d\xi \qquad (82)$$

After integrating by parts, T_F may be written in a more convenient manner as

$$T_F = -(F_A + F_{cor})(v'\delta v' + w'\delta w') \qquad (83)$$

where

$$F_A = \int_x^R mx\, d\xi \qquad (84)$$

$$F_{cor} = \int_x^R 2m\dot{v}\, d\xi \qquad (85)$$

The terms associated with F_A reflect the centrifugal stiffening effects on the flap and lag equations while the terms associated with F_{cor} reflect the nonlinear Coriolis damping effects in those equations. The terms associated with F_A and F_{cor} are added to $T_{v_2'}$ and $T_{w_2'}$ which allows the linear contribution to the kinetic energy variation to be written as

$$\delta T_{lin} = \int_0^R \{\delta\dot{\hat{u}}_i m_{ij} \dot{\hat{u}}_j + \delta\dot{\hat{u}}_i c_{ij} \hat{u}_j + \delta\hat{u}_i k_{ij} \hat{u}_j)\, dx \qquad (86)$$

A more useful form of the above expression is obtained by integrating the variation in kinetic energy by parts over time. This can be done because in applying Hamilton's principle the variation in kinetic energy will be integrated in time. By temporarily switching the order of integration, the integration by parts can be performed.

$$\int_{t_1}^{t_2} \int_0^1 \delta\dot{u}_i m_{ij} \dot{u}_j dx\, dt = \int_0^1 \int_{t_1}^{t_2} \delta\dot{u}_i m_{ij} \dot{u}_j dt\, dx =$$

$$\int_0^1 (\delta u_i m_{ij} \dot{u}_j \Big|_{t_1}^{t_2} - \int_{t_1}^{t_2} \delta u_i m_{ij} \ddot{u}_j\, dt)\, dx =$$

$$-\int_{t_1}^{t_2} \int_0^1 \delta u_i m_{ij} \ddot{u}_j\, dx\, dt \qquad (87)$$

After a similar operation on the damping term of Eqn. 86, the linear variation of kinetic energy becomes

$$\delta T_{lin} = \int_0^R \delta\hat{u}_i \{m_{ij} \ddot{\hat{u}}_j + c_{ij} \dot{\hat{u}}_j + k_{ij} \hat{u}_j\}\, dx \qquad (88)$$

APPENDIX B
IMPLEMENTATION

Introduction

The present formulation is implemented as a beam finite element. Many past analyses for rotating blades have used this approach, but the order of polynomials used to approximate the displacements has varied. The analysis of Kosmatka (1986) uses a quadratic torsion and axial approximation along with cubic Hermitian polynomials for bending. This set of assumptions provides the same level of accuracy in the torsion and axial deformations as in the bending deformations. The analyses of Hong and Chopra (1985a, 1985b) and Smith and Chopra (1991) use similar displacement polynomials, but with a cubic axial approximation, developed as a mean for improving the axial mode predictions.

A higher order element capability was developed for the dynamic analysis of beams in the GRASP code (Hodges *et. al.*, 1990). In this code the user could independently increase the order of polynomial approximation of each displacement to match the physical characteristics of the beam. This is the so-called p-version finite element approach, and seems ideally suited for application to analysis of elastically-coupled beams because of the dramatic influence elastic couplings have on beam flexibility in some displacement modes. The study of Hinnant (1989) demonstrated that, given proper modeling of the beam geometry, there is also substantial savings to be gained by use of p-version elements in terms of total number of degrees of freedom required to obtain an accurate solution.

Finite Element Implementation

The linear parts of the strain and kinetic energies as defined in Eqns. 66 and 88 are used to develop a p-version beam finite element. The continuous displacements which appear in these expressions are u, v, w, and ϕ, and are functions of both x and time. The continuous problem is discretized by introducing discrete degrees of freedom q_i which are related to the continuous displacements according to

$$u = \sum_{i=1}^{P_u} N_i^u q_i^u \qquad (89)$$

$$v = \sum_{i=1}^{P_v} N_i^v q_i^v \qquad (90)$$

$$w = \sum_{i=1}^{P_w} N_i^w q_i^w \qquad (91)$$

$$\phi = \sum_{i=1}^{P_\phi} N_i^\phi q_i^\phi \qquad (92)$$

where N_i are shape functions defined later in this section. Substitution of these equations into Eqns. 66 and 88 gives the strain and kinetic energies in terms of the discrete degrees of freedom. The virtual energy expression defined in Eqn. 1 may also be written in discretized form as

$$\delta\Pi = \int_{t_1}^{t_2} \left[\sum_{i=1}^{N} (\delta U_i - \delta T_i)\right] dt \qquad (93)$$

where N is the number of spatial elements used to discretize the elastic blade. Each element is represented using the discrete displacements as

$$\delta U - \delta T = \delta q_i^T \{M_{ij}\ddot{q}_j + C_{ij}\dot{q}_j + K_{ij}q_j\} \quad (94)$$

where the element mass, damping, and stiffness matrices are defined by

$$M_{ij} = \int_0^R B_{ik} m_{kl} B_{lj}\, dx \quad (95)$$

$$C_{ij} = \int_0^R B_{ik} c_{kl} B_{lj}\, dx \quad (96)$$

$$K_{ij} = \int_0^R (A_{ik} k_{kl} A_{lj}\, dx - B_{ik} k_{kl} B_{lj})\, dx \quad (97)$$

where $B_{ik} = B_{lj}^T$ and $A_{ik} = A_{lj}^T$. B is a matrix of shape functions and shape function derivatives which satisfies the relationship

$$u_i = (D_T)_{ij}[\hat{u}_j] = (D_T)_{ij}[H_{jk}q_k] = B_{ik}q_k \quad (98)$$

where $\hat{u}_j$ is a vector of the continuous degrees of freedom u, v, w, and ϕ. D_T is a matrix of derivative operators associated with the kinetic energy formulation and H is a matrix of shape functions whose arrangement depends on the selection of discrete variables in q, and satisfies Eqns. 89-92. The definition of A_{ij} is similar to that of B_{ij} except that it is associated with the strain energy formulation. Thus, B may be replaced by A and subscripts of T may be replaced by V in Eqn. 98.

The discrete degrees of freedom are divided into two sets, external and internal. There are twelve external degrees of freedom which have physical significance as the displacements and rotations associated with the ends of the beam finite element (six on each end). These deformations are depicted in Fig. 10. The shape functions for N_i^u and N_i^ϕ are identical and have C^0-type continuity. There are two well-known linear

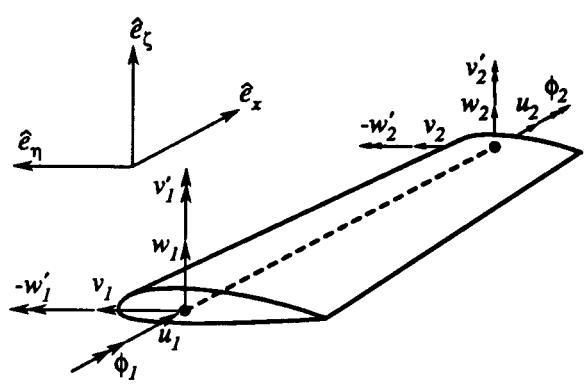

Figure 10: Beam element showing external discrete degrees of freedom.

polynomials used to define this set:

$$N_1^0 = 1 - \frac{x}{l} \quad (99)$$

$$N_2^0 = \frac{x}{l} \quad (100)$$

where $N_i^u = N_i^\phi = N_i^0$. The shape functions N_i^v and N_i^w require C^1-type continuity. These shape functions are given by:

$$N_1^1 = 2\frac{x^3}{l^3} - 3\frac{x^2}{l^2} + 1 \quad (101)$$

$$N_2^1 = \frac{x^3}{l^2} - 2\frac{x^2}{l} + x \quad (102)$$

$$N_3^1 = -2\frac{x^3}{l^3} + 3\frac{x^2}{l^2} \quad (103)$$

$$N_4^1 = \frac{x^3}{l^2} - \frac{x^2}{l} \quad (104)$$

where $N_i^v = N_i^w = N_i^1$.

The internal degrees of freedom have no physical significance, but are simply coefficients of the higher order shape functions. The internal degrees of freedom serve to increase the accuracy of the transformation from the discrete problem having a finite number of degrees of freedom to the continuous problem having an infinite number of degrees of freedom. In the present formulation, the number of internal degrees of freedom is limited to four for the C^0-type displacements, and to two for the C^1-type displacements. There are, therefore, a total of six internal shape functions associated with each continuous displacement u, v, w, and ϕ. The additional C^0-type shape functions for u and ϕ are

$$N_3^0 = \sqrt{3}\left(\frac{x^2}{l^2} - \frac{x}{l}\right) \quad (105)$$

$$N_4^0 = \sqrt{5}\left(-2\frac{x^3}{l^3} + 3\frac{x^2}{l^2} - \frac{x}{l}\right) \quad (106)$$

$$N_5^0 = \sqrt{7}\left(5\frac{x^4}{l^4} - 10\frac{x^3}{l^3} + 6\frac{x^2}{l^2} - \frac{x}{l}\right) \quad (107)$$

$$N_6^0 = -42\frac{x^5}{l^5} + 105\frac{x^4}{l^4} - 90\frac{x^3}{l^3} + 30\frac{x^2}{l^2} - 3\frac{x}{l} \quad (108)$$

These shape functions are derived by Hinnant (1989) based on satisfaction of two requirements: first, the higher order shape functions must be zero at the element boundaries, and second, they must be orthogonal with respect to their first derivative. The additional C^1-type shape functions for v and w are given by

$$N_5^1 = \sqrt{5}\left(\frac{x^4}{2l^4} - \frac{x^3}{l^3} + \frac{x^2}{2l^2}\right) \quad (109)$$

$$N_6^1 = \sqrt{7}\left(-\frac{x^5}{l^5} + 5\frac{x^4}{2l^4} - 2\frac{x^3}{l^3} + \frac{x^2}{2l^2}\right) \quad (110)$$

The derivation of these higher-order polynomials is similar to that of the C^0-type polynomials, only the functions must also have zero slope at the element boundaries, and must be orthogonal in their second derivative.

The arrangement of shape functions in the matrix of shape functions H depends on the arrangement of discrete degrees of freedom in q. To facilitate the element assembly process, the discrete unknowns were grouped with the first twelve external nodes together, followed by the twelve internal nodes ($4u$, $2v$, $2w$, and

4ϕ). The arrangement of the vector of discrete degrees of freedom is given as

$$q = \left\{ \begin{array}{c} u_1 \\ v_1 \\ w_1 \\ \phi_1 \\ -w_1' \\ v_1' \\ u_2 \\ v_2 \\ w_2 \\ \phi_2 \\ -w_2' \\ v_2' \\ u_3 \\ u_4 \\ u_5 \\ u_6 \\ v_3 \\ v_4 \\ w_3 \\ w_4 \\ \phi_3 \\ \phi_4 \\ \phi_5 \\ \phi_6 \end{array} \right\} \tag{111}$$

Before the symbolic integrations of Eqns. 95-97 can be carried out, the mass, damping, and stiffness cross section matrices (m, c, k, and k) must be defined as polynomials in x. The cross section terms are functions of x because of the presence of the twist angle in many of the terms, which is itself a function of x. In the present formulation, it is desired to have the capability of accounting for changes in cross section properties beyond that due to twist, such as taper, for example. A beam element does not allow for such effects directly, so a quadratic polynomial curve fit was adapted to increase the accuracy of the element for changes in cross section properties along its length.

The mass, damping, and stiffness matrices as given by Eqns. 95-97 were symbolically integrated to obtain 24 x 24 element matrices. These matrices were implemented in an analysis to determine the modes and frequencies of highly-twisted elastically-coupled rotor blades. As part of this implementation, the displacement approximations could be chosen for each continuous displacement independently. The external displacements represent the minimum number of degrees of freedom for each element, while the maximum is given by use of all twelve internal degrees of freedom. Any choice between 12 and 24 degrees of freedom per element could be accomodated in the analysis. The notation adopted for the present formulation is to select a "p" value which represents the number of internal degrees of freedom associated with a particular displacement. For example, an element with $p_u = 1$ and $p_\phi = 1$ uses the basic cubic hermitian polynomial approximation in bending (no internal degrees of freedom) and quadratic polynomial approximations in the axial and torsion displacements. This particular example happens to represent the most common approximation used in finite element rotor blade dynamic analysis because it gives an equivalent level of approximation in all displacement modes.

REPORT DOCUMENTATION PAGE

Form Approved
OMB No. 0704-0188

Public reporting burden for this collection of information is estimated to average 1 hour per response, including the time for reviewing instructions, searching existing data sources, gathering and maintaining the data needed, and completing and reviewing the collection of information. Send comments regarding this burden estimate or any other aspect of this collection of information, including suggestions for reducing this burden, to Washington Headquarters Services, Directorate for Information Operations and Reports, 1215 Jefferson Davis Highway, Suite 1204, Arlington, VA 22202-4302, and to the Office of Management and Budget, Paperwork Reduction Project (0704-0188), Washington, DC 20503.

1. AGENCY USE ONLY *(Leave blank)*

2. REPORT DATE
January 1994

3. REPORT TYPE AND DATES COVERED
Technical Memorandum

4. TITLE AND SUBTITLE
Dynamic Analysis of Pretwisted Elastically-Coupled Rotor Blades

5. FUNDING NUMBERS
WU 505-63-50-15

6. AUTHOR(S)
Mark W. Nixon and Howard E. Hinnant

7. PERFORMING ORGANIZATION NAME(S) AND ADDRESS(ES)
NASA Langley Research Center
Hampton, VA 23681-0001

8. PERFORMING ORGANIZATION REPORT NUMBER

9. SPONSORING/MONITORING AGENCY NAME(S) AND ADDRESS(ES)
National Aeronautics and Space Administration
Washington, DC 20546-0001

10. SPONSORING/MONITORING AGENCY REPORT NUMBER
NASA TM-109070

11. SUPPLEMENTARY NOTES
Presented at the 1992 ASME Winter Annual Meeting, November 8-13, 1992, Anaheim, CA.
Mark W. Nixon and Howard E. Hinnant employed by U.S. Army Vehicle Structures Directorate, NASA Langley Research Center, Hampton, Virginia.

12a. DISTRIBUTION/AVAILABILITY STATEMENT
Unclassified - Unlimited

Subject Category 39

12b. DISTRIBUTION CODE

13. ABSTRACT *(Maximum 200 words)*

This paper addresses the accuracy of using a one-dimensional analysis to predict frequencies of elastically-coupled highly-twisted rotor blades. Degrees of freedom associated with shear deformation are statically condensed from the formulation, so the analysis uses only those degrees of freedom associated with classical beam theory. The effects of cross section deformation (warping) are considered, and are shown to become significant for some types of elastic coupling. Improved results are demonstrated for highly-coupled blade structures through account of warping in a local cross section analysis, without explicit inclusion of these effects in the beam analysis. A convergence study is also provided which investigates the potential for improving efficiency of elastically-coupled beam analysis through implementation of a p-version beam finite element.

14. SUBJECT TERMS
Elastic tailoring, composite structures, rotary wing dynamics, composite rotor blades, anisotropic beams

15. NUMBER OF PAGES
17

16. PRICE CODE
A03

17. SECURITY CLASSIFICATION OF REPORT
Unclassified

18. SECURITY CLASSIFICATION OF THIS PAGE
Unclassified

19. SECURITY CLASSIFICATION OF ABSTRACT

20. LIMITATION OF ABSTRACT